

THE POLARITY DEPENDENT EFFECT OF GYROVISCOSITY ON THE FLOW SHEAR STABILIZED RAYLEIGH-TAYLOR INSTABILITY

E. L. Ruden

Air Force Research Laboratory, Directed Energy Directorate, Kirtland AFB, US

The general linear dispersion relation is reviewed for incompressible fluid modes with wave numbers transverse to the magnetic field in a magnetically accelerated finite Larmor radius plasma where the unperturbed density and fluid velocity in the wave number direction vary in the direction of acceleration. Stability criteria are derived and unstable growth rate diagrams plotted for the combined Rayleigh-Taylor/Kevin-Helmholtz modes for various two and three region piecewise uniform cases.

The effect of gyroviscosity on large wave number stability is shown to differ if the direction of the magnetic field is reversed, all else being equal, being either stabilizing or destabilizing depending on this direction. This implies an electrode polarity dependence for magnetically accelerated plasmas with sheared flow, such as is found in plasma foci. This mechanism is suggested as a possible reason why the plasma focus has superior performance when the center conductor is the anode.

Given a central anode, a maximum Bt product is derived for stable large wave numbers for given current waveform, where B is the driving magnetic field magnitude and t is the current rise timescale. This implies critical constraints on energy and power scaling, though strategies for mitigating the constraints are discussed, such as applying an exponentially increasing current waveform. Ultimately, this may lead to higher performance for plasma foci and related devices such as flow shear stabilized z-pinch.

1. Model

We assume a perfectly conducting isothermal z invariant plasma with a magnetic field of magnitude B in the unit vector \mathbf{z} direction, and a uniform gravitational field of magnitude g in the $-\mathbf{x}$ direction. For incompressible motion confined to the $x - y$ plane, the MHD equation of motion supplemented by the isothermal FLR stress tensor $\mathbf{\Pi}$ (Hazeltine and Meiss[1] Eq. 123), along with the equations of continuity and state are

$$\begin{aligned} \rho \partial \mathbf{v} / \partial t + \rho (\mathbf{v} \cdot \nabla) \mathbf{v} &= -\nabla p^* - g \rho \mathbf{x} - \nabla \cdot \mathbf{\Pi} & \partial \rho / \partial t + \nabla \cdot (\rho \mathbf{v}) &= 0 \\ \nabla \cdot \mathbf{v} &= 0 & p^* \equiv k_B T \rho / m_i + B^2 / (2\mu_0) & \nu = k_B T_i / (2ZeB) & T \equiv (T_i + ZT_e) \\ \Lambda_x \equiv -(\nabla \cdot \mathbf{\Pi}) \cdot \mathbf{x} &= \frac{\partial}{\partial x} \left[\nu \rho \left(\frac{\partial v_y}{\partial x} + \frac{\partial v_x}{\partial y} \right) \right] - \frac{\partial}{\partial y} \left[\nu \rho \left(\frac{\partial v_x}{\partial x} - \frac{\partial v_y}{\partial y} \right) \right] \\ \Lambda_y \equiv -(\nabla \cdot \mathbf{\Pi}) \cdot \mathbf{y} &= -\frac{\partial}{\partial y} \left[\nu \rho \left(\frac{\partial v_y}{\partial x} + \frac{\partial v_x}{\partial y} \right) \right] - \frac{\partial}{\partial x} \left[\nu \rho \left(\frac{\partial v_x}{\partial x} - \frac{\partial v_y}{\partial y} \right) \right] \end{aligned} \quad (1)$$

\mathbf{v} , ρ , $\mathbf{\Lambda}$, m_i , μ_0 , k_B , T_i , T_e , e , and Z are the fluid velocity, density, FLR force density vector, ion mass, free space permeability, Boltzmann constant, ion and electron temperatures, elementary charge, and mean ionization level, respectively.

The equilibrium state of interest has $\mathbf{v} = v_{y0}(x) \mathbf{y}$, $\rho = \rho_0(x)$, $\mathbf{B} = B_0(x) \mathbf{z}$, and $\nu = \nu_0(x)$. Assuming first order perturbations (terms with subscript 1) with $\exp(i\omega t +iky)$ dependence, the resultant dispersion relation is

$$\begin{aligned} D \left[(\rho_0 \omega^{*2} - 2k\nu_0 \omega^* D\rho_0) D \left(\frac{u}{\omega^*} \right) + 2k\rho_0 (k^2\nu_0 u - (D\nu_0) Du - (i\nu_1) D\omega^*) \right] \\ = \frac{k^2 g u}{\omega^*} D\rho_0 + 2k^3 \nu_0 \rho_0 Du + k^2 \rho_0 u \omega^* & (i\nu_1) = \frac{-S}{(1-S)\rho_0 D\omega^*} \times \\ \left[\frac{\rho_0 \omega^{*2}}{k} D \left(\frac{u}{\omega^*} \right) - 2(Du) D(\nu_0 \rho_0) + \rho_0 \nu_0 (k^2 u - D^2 u) + \left(\frac{k k_B T}{m_i} + \nu_0 D\omega^* \right) \frac{u D\rho_0}{\omega^*} \right] \\ S \equiv \frac{\beta_i m_i}{4ZeB_0} \frac{D\omega^*}{k} & \beta_i \equiv \frac{\rho_0 k_B T_i / m_i}{B_0^2 / 2\mu_0} & D \equiv \frac{\partial}{\partial x} & \omega^* \equiv \omega + kV & u \equiv v_{x1} & V \equiv v_{y0} \end{aligned} \quad (2)$$

Assuming $|S| \ll 1$, within any range of x with uniform ρ_0, ν_0 , and $s = DV$, Eqs. 2 reduce to

$$D^2u - k^2u = 0 \quad u = \text{constant} \times \exp(i\omega t +iky \pm kx) \quad (3)$$

For cases with a discontinuous change in ρ_0, DV , and/or ν_0 at $x = x_i$, the first of Eqs. 2 may be integrated across the boundary to obtain jump conditions to match solutions on each side. Such conditions between two regions with different uniform values of ρ_0, ν_0 , and s are, for $|S| \ll 1$,

$$\begin{aligned} \Delta_i [\rho_0 (\omega^{*2} Du + (2k^2 \nu_0 \omega^* - s\omega^* - kg) ku) / \omega^*] &= 0 \\ \Delta_i [V] = 0 \quad \Delta_i [u] = 0 \quad \Delta_i (f(x)) &\equiv \lim_{\epsilon \rightarrow 0} (f(x_i + \epsilon) - f(x_i - \epsilon)) \end{aligned} \quad (4)$$

3. Case I: Two semiinfinite regions with different uniform ρ_0, s , and ν_0

We assume two semiinfinite regions separated at $x = 0$ with

$$\begin{aligned} \rho_0 = \rho_1 \quad V = s_1 x \quad \nu_0 = \nu_1 \quad \text{if } x < 0 \\ \rho_0 = \rho_2 \quad V = s_2 x \quad \nu_0 = \nu_2 \quad \text{if } x \geq 0 \end{aligned} \quad (5)$$

where $\rho_1, \rho_2, s_1, s_2, \nu_1$, and ν_2 are constants (subscript 1 now refers to region 1). Equations 3 and Eqs. 4 imply, for bound solutions,

$$\omega^2 - (2k^2 \nu^* - s^*) \omega + kg^* = 0 \quad \nu^* = \frac{\nu_2 \rho_2 - \nu_1 \rho_1}{\rho_1 + \rho_2} \quad s^* = \frac{s_2 \rho_2 - s_1 \rho_1}{\rho_1 + \rho_2} \quad g^* = g \frac{\rho_2 - \rho_1}{\rho_1 + \rho_2} \quad (6)$$

The condition for instability, implying maximum growth rate $\gamma = \max(-\text{Im } \omega)$, is

$$J^* > \frac{(1 - G^* K^2)^2}{2K} \rightarrow \Gamma = \sqrt{1 - \frac{(1 - G^* K^2)^2}{2J^* K}} \quad J^* \equiv \frac{g^*}{s^{*2} d} \quad K \equiv 2kd \quad G^* \equiv \frac{\nu^*}{2s^* d^2} \quad \Gamma \equiv \frac{\gamma}{\sqrt{g^* k}} \quad (7)$$

Here, d is the half-thickness of the plasma layer intended to be modeled (included for comparison with Case II). An R-T relevant configuration is one for which $\rho_2 > \rho_1$, implying positive J^* . G^* may be of either sign regardless of the relative magnitudes of ρ_1 and ρ_2 .

We see from Eqs. 7 that there is no global stability (ie., for all K) if $J^* > 0$ and $G^* > 0$, and gyroviscosity suppresses the stabilizing influence of flow shear in the vicinity of $K = \sqrt{G^*}$. However, from differential extremum analysis for a given $G^* < 0$, the K that requires the smallest J^* to be stable is $K_{\text{crit}} = 1/\sqrt{-3G^*}$, and the global stability criterion is

$$J^* \leq \begin{cases} 8\sqrt{-G^*/27} & \text{if } G^* < 0 \\ 0 & \text{if } G^* \geq 0 \end{cases} \quad (8)$$

4. Case II: Two regions with opposing velocities separated by a third region with a sheared transitional velocity profile

We now assume three regions of uniform ρ_0 and ν_0 with equilibrium properties identified by subscripts 1, 2, and 3. We restrict uniform flow shear to the intermediate region of thickness $2d$, and drop the “*” superscripts used to generalize the results. In equilibrium,

$$\begin{aligned} \rho_0 = \rho_1 \quad V = -sd \quad \nu_0 = \nu_1 \quad \text{if } x < -d \\ \rho_0 = \rho_2 \quad V = sx \quad \nu_0 = \nu_2 \quad \text{if } -d < x < +d \\ \rho_0 = \rho_3 \quad V = +sd \quad \nu_0 = \nu_3 \quad \text{if } x > +d \end{aligned} \quad (9)$$

Equations 3, Eqs. 4, and Eqs. 9 imply, for bound solutions,

$$\begin{aligned} \frac{(1 - \epsilon_3)(1 + \Omega_+^2) - 2K(G_2 - \epsilon_3 G_3)\Omega_0\Omega_+ + 2\Omega_0\Omega_+/K}{1 - \epsilon_3 - (1 + \epsilon_3)\Omega_+^2 - 2K(G_2 - \epsilon_3 G_3)\Omega_0\Omega_+ + 2\Omega_0\Omega_+/K} &= \frac{1 - \epsilon_1 + (1 + \epsilon_1)\Omega_-^2 - 2K(G_2 - \epsilon_1 G_1)\Omega_0\Omega_- + 2\Omega_0\Omega_-/K}{(1 - \epsilon_1)(1 - \Omega_-^2) - 2K(G_2 - \epsilon_1 G_1)\Omega_0\Omega_- + 2\Omega_0\Omega_-/K} e^{2K} \\ \Omega &\equiv \frac{\omega}{\sqrt{gk}} \quad \Omega_0 \equiv \sqrt{\frac{K}{2J}} \quad \Omega_{\pm} \equiv \Omega \pm \Omega_0 \quad K \equiv 2kd \quad J \equiv \frac{g}{s^2 d} \quad G_i \equiv \frac{\nu_i}{2sd^2} \quad \epsilon_i \equiv \frac{\rho_i}{\rho_2} \end{aligned} \quad (10)$$

This expands into a quartic polynomial in Ω , which we solve numerically. Figure 1 plots the stability boundaries and $\Gamma = 1$ contours for various G_2 with $\epsilon_1 = \epsilon_3 = 0$. This represents a plasma layer accelerated by a B field. G_1 and G_3 have no effect since G_i drops out if $\epsilon_i = 0$. Equation 8 with $G^* = G_2$ is seen here to suffice as the large K stability criterion for $J \lesssim 0.3$.

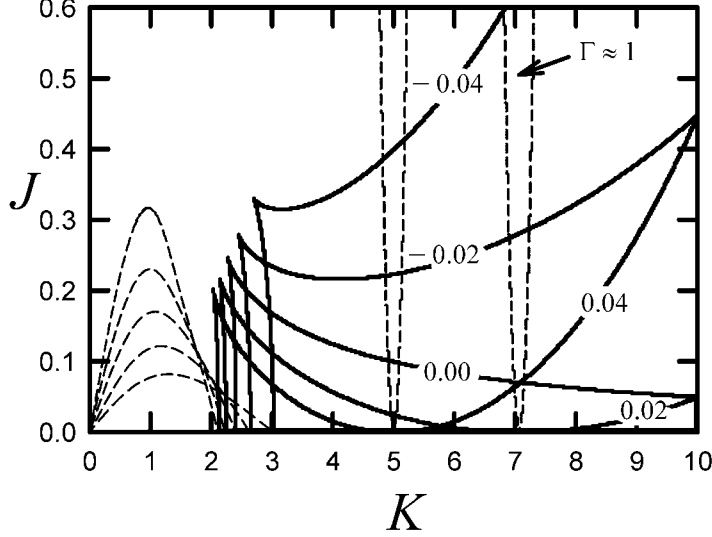


Fig. 1 Stability boundaries (solid) and $\Gamma = 1$ contours (dashed) for Case II with $\epsilon_1 = \epsilon_3 = 0$ for various G_2 values (labeled).

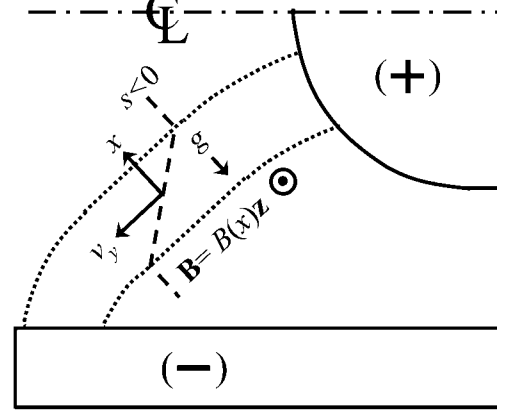


Fig. 2 Case II applied to plasma focus. The \mathbf{B} vector is pointing out of the page.

5. Plasma focus application

A PF consists of pair of truncated coaxial electrodes with a gas prefill. Voltage applied across the electrodes creates a current sheath in the medium which forms a magnetic pressure driven mass accreting shocked layer that propagates primarily in the axial direction until the end of the inner electrode is reached. Thereafter, the inner part of the shocked layer bends radially inward, implodes, and forms a z-pinch on axis. The axial momentum of plasma accreted during the earlier phase is retained during implosion phase, while plasma accreted during the implosion is given less axial momentum. The resultant characteristic flow shear factor may be expressed as $s = \pm\eta V_0/2d$, where V_0 is the speed of the current sheath, and $2d$ is the shocked layer thickness. η is the shearing efficiency, with an optimally designed system having a value close to unity. Figure 2 illustrates Case II geometry applied to the accretion phase for a PF with a central anode. It is not to scale, and the shape of the electrodes is chosen simply to make the figure compact. The axes and dashed line represent the coordinate system and a negative s velocity profile, respectively. The origin is tied to a fluid element at intermediate depth within the accretion layer. If the magnetic field were reversed (into the paper), $s > 0$ would represent the velocity profile that results from PF dynamics, and the center conductor would be the cathode.

We estimate effective Case II model parameters using the planar “snow plow” model[2] of plasma accretion in conjunction with a more detailed planar model[3] that provides self-similar solutions to the accretion layer’s density profile. The former assumes that the layer is thin enough to neglect it’s internal structure for the purposes of overall momentum and mass conservation, while the latter applies to cases where a thin current sheath propagates through an initially cold uniform gas according a power law or, alternately, a exponential in time. We have, then,

$$\frac{B_0^2}{2\mu_0} = \frac{d}{dt} (\sigma V_0) \quad \sigma = \rho_f L \quad V_0 = \frac{dL}{dt} \quad L = a \frac{t^n}{n} \quad (n \geq 1) \quad \text{or} \quad L = g_0 t_0^2 \exp\left(\frac{t}{t_0}\right) \quad (11)$$

where σ is the layer’s mass per unit area, ρ_f is the prefill density, $L = L(t)$ is the distance propagated by the current sheath, and B_0 is the magnetic field magnitude driving the

layer. Near the current sheath $\rho \approx \rho_f N_1 (x/L)^{-\alpha}$, where x is distance ahead of the sheath, $\alpha = 2(n-1)/(n(\gamma+2)-2)$, γ is the specific heats ratio, and $N_1 = N_1(n, \gamma)$ is determined numerically. The exponential case corresponds to $n \rightarrow \infty$. d is chosen to be the distance in front of the sheath that our ρ approximation must be integrated to equal $\sigma/2$. $B_0^2/2\mu_0$ and $\sigma/(2d)$ are taken to be the characteristic plasma pressure and density, respectively. T is determined from the ideal gas law. $T_i = T_e = T/(1+Z)$ and $\nu_2 = k_B T_i/(2ZeB_0)$ are assumed. Our stability criteria and least stable mode in general, and for an ideal gas with $n = 2$ (linear B_0 rise) and exponential L (and therefore B_0) in particular are, respectively,

$$\begin{aligned} \frac{eZ(1+Z)B_0 t}{\eta^3 m_i} &= \frac{eZ(1+Z)L\sqrt{2\mu_0 n(2n-1)\rho_f}}{\eta^3 m_i} < \frac{4n^2(2n-1)}{27(n-1)^2} \left(\frac{2N_1}{1-\alpha}\right)^{2/(1-\alpha)} & K_{\text{crit}} &= \frac{2n\eta^2}{9(n-1)} \left(\frac{2N_1}{1-\alpha}\right)^{1/(1-\alpha)} \\ \frac{eZ(1+Z)B_0 t}{\eta^3 m_i} &= \frac{2eZ(1+Z)L}{\eta^3 m_i} \sqrt{3\mu_0 \rho_f} < 12777. & K_{\text{crit}} &= 11.9\eta^2 \quad (n=2, \gamma=\frac{5}{3}) \\ \frac{eZ(1+Z)B_0 t_0}{\eta^3 m_i} &= \frac{eZ(1+Z)L}{\eta^3 m_i} \sqrt{2\mu_0 \rho_f} < 767. & K_{\text{crit}} &= 13.4\eta^2 \quad (\text{exp current}, \gamma=\frac{5}{3}) \end{aligned} \quad (12)$$

The values of B_0 and L in terms of machine parameters are still vague at this point. A conservative choice for B_0 would be B at the radius R_1 of the center conductor, given machine current I and Ampere's law. Meanwhile, optimizing η entails balancing the mass accreted during the axial acceleration phase with that of the radial implosion phase. This suggests that the inner electrode length should be comparable to its radius. Given these assumptions, an interesting result is obtained by constraining the various cases' stability criteria by empirical scaling constant C for D₂ PF optimized for maximum neutron yield[4],

$$\begin{aligned} C &= I / \left(R_1 \sqrt{\rho_f} \right) = 5.79 \times 10^8 \text{ A}\cdot\text{m}^{\frac{1}{2}}\cdot\text{kg}^{-\frac{1}{2}} & B_0 &= \mu_0 I / 2\pi R_1 & L &= 2R_1 \\ R_1 &= \frac{\sqrt{\mu_0} Ct}{4\pi\sqrt{2n(2n-1)}} & I/\eta^3 &< \frac{n\sqrt{2n(2n-1)}}{27(n-1)^2} \left(\frac{2N_1}{1-\alpha}\right)^{2/(1-\alpha)} \frac{Cm_i}{eZ(1+Z)\sqrt{\mu_0}} & & (13) \\ R_1 &= \frac{\sqrt{\mu_0} Ct}{8\pi\sqrt{3}} = 1.49 \times 10^4 t \frac{\text{m}}{\text{s}} & I/\eta^3 &< 184.3 \frac{m_i C}{eZ(1+Z)\sqrt{\mu_0}} = 2.0 \text{ MA} & (\text{linear}) \\ R_1 &= \frac{\sqrt{\mu_0} Ct_0}{4\pi\sqrt{2}} = 3.65 \times 10^4 t_0 \frac{\text{m}}{\text{s}} & I/\eta^3 &< 271.2 \frac{Cm_i}{eZ(1+Z)\sqrt{\mu_0}} = 2.9 \text{ MA} & (\text{exp}) \end{aligned}$$

Note, if $m_i C / (Z(1+Z))$ is increased for other applications, a higher critical current is implied.

The above assumes $|S| \ll 1$ (Eqs. 2). For an ideal gas, given the rest of our assumptions, $|S| = 5.2 \times 10^{-3}/\eta^2$ and $|S| = 9.9 \times 10^{-3}/\eta^2$ for a linear and exponential current ramp at the stability threshold, respectively. $|S| \ll 1$ is valid, therefore, for $\eta \sim 1$.

Equations 13 do not necessarily imply that a neutron optimized D₂ PF operating at greater than the critical current will emit fewer neutrons than one operating at that current. If that were the case, conventional (unstable) z-pinchs without sheared flow would not work as they do. A more reasonable prediction is that there will be a diminished return on increasing the current. The I^4 neutron production scaling law may break down, for example. Furthermore, the presented model involves crude approximations of PF dynamics, so the ultimate current threshold may be significantly different. To test the theory empirically does not necessarily require currents exceeding the neutron optimized limits of Eqs. 13. The more general $B_0 t$ thresholds of Eqs. 12 may be reached at lower current by reducing the anode diameter.

References

- [1] R. D. Hazeltine and J. D. Meiss, *Plasma Confinement* (Addison-Wesley, Redwood, CA, 1992), p. 219.
- [2] N. A. Krall and A. W. Trivelpiece, *Principles of Plasma Physics* (McGraw-Hill, New York, NY, 1973), pp. 124–126.
- [3] S. M. Gol'berg and A. L. Velikovich, *Phys. Fluids B* **5**, 1164 (1993).
- [4] S. Lee and A. Serban, *IEEE Trans. on Plasma Sci.* **24**, 1101 (1996).